Isobar-width effects in the coupling of nucleon to isobar channels

P. González* and E. L. Lomon
Center for Theoretical Physics, Laboratory for Nuclear Science and Department of Physics, Massachusetts Institute of Technology, Cambridge, Massachusetts 02139
(Received 26 February 1986)

The investigation of the effects of isobar coupling to two-nucleon channels has been extended to include additional physical features. A new code discretizes the mass distribution of the isobar widths and treats each mass as a separate channel. This allows the treatment of width in the presence of coupling by transition potentials, in addition to the previously permitted boundary coupling. It also produces the S-matrix components required to describe the many-body final-state distributions. When indicated by the one-pion-exchange coupling strength new isobar channels are included. The new results for nucleon-nucleon scattering fit the data better, starting from more realistic models. The observed $^1D_2$ and $^3F_3$ structures are well understood as coupled-channel effects, without exotic-quark contributions. The existence of a structure in the $^3P_0$ channel depends on the amount of inelasticity, which differs among the phase shift solutions. The energy dependence seen in recent analyses, of the $^3P_2$ phase shift near $T_L=800$ MeV, is shown to be a consequence of the isobar channel coupling. Improved models obtained for the $^1S_0$ and $^3S_1$-$^3D_1$ channels are being developed. They are important to accurately extrapolate those phases to higher energies where six-quark effects are expected.

I. INTRODUCTION

Data from medium-energy accelerators have provided important information about two-hadron systems, including new structures in nucleon-nucleon scattering and accurate deuteron form factors in an extended momentum-transfer range. In nucleon-nucleon scattering the first isobar channel, the $N\Delta$, has a threshold at a laboratory beam energy $T_L=630$ MeV (lower when the Δ width is included). Consequently, the coupling of isobar channels is of great importance for $T_L \geq 400$ MeV and must be considered in the present medium-energy range of several GeV. The explicit treatment of the isobar-channel effects is necessary to the understanding of the growing amount of pion production data.[1]

For $T_L \geq 1.5$ GeV it is expected that quark degrees of freedom will have a significant role.[2] In order to distinguish their effects from conventional hadronic effects, the behavior of the coupled hadronic channels must be well understood. For instance, the $^1D_2$ and $^3F_3$ two-nucleon structures,[3] which have been suggested to represent six-quark states,[4] have been shown to be predicted by coupling to $N\Delta$ channels.[5-8] Furthermore, the prediction of the size of observable effects of resonances caused by exotic-quark states[9,10] requires a coupled-channel model extrapolation of the background phase parameters.

Previous coupled-channel calculations[5-8] have been successful in predicting many of the features of intermediate-energy nucleon-nucleon reactions, as well as of some meson-baryon reactions.[11-15] However, this extant work falls short of the realism demanded by the present data or the completeness required to satisfy the objectives mentioned above. In some cases the long-range interaction is missing or inadequate,[11-15] while in others the short-range interaction is not sufficiently realistic.[6-8] Sometimes the decay width of the isobars is neglected. In many cases some significant coupled channels are omitted. In Ref. 5 either the effect of the isobar decay width or of the transition potential is taken into account, but not both together. Also in Ref. 5, significant coupled channels are omitted from a few partial waves.

The present work is an extension of that of Ref. 5, for several of the most interesting nucleon-nucleon partial waves, which overcomes the width restriction and includes more significant channels. In Ref. 5 the short-range interaction is described by an energy-independent boundary condition at $r_0 \simeq \frac{1}{2} m_\pi^{-1}$:

$$r_0 \left[\frac{d\psi^\alpha}{dr} \right]_{r_0} = f \psi^\alpha(r_0) , \tag{1}$$

where f is a square matrix of constant coefficients and $\psi^\alpha(r)$ is a column matrix of coupled-channel wave functions with the strong-quantum-number list denoted by α (α denotes J, S, T, and P for the systems discussed in this article). This boundary condition has been shown[16] to represent the strong, nonlocal, short-range interaction below the energy of states internal to r_0. Furthermore, it is easily extended[2] to treat the effects of quark-gluon internal states by the addition of simple, real poles of positive residue to the energy-independent f.

Outside of r_0, the interaction in the nucleon sector is taken to be the Feshbach-Lomon potential[17] which includes the contribution of two-pion exchange as well as of single π, η, ρ, and ω exchange. The transition potentials from the NN sector to the $N\Delta$, $\Delta\Delta$, and $NN^*(1440)$ sectors are those determined from one-pion exchange and, sometimes, a phenomenological two-pion range potential (which may also simulate η, ρ, and ω exchange).

When the transition potentials are neglected the coupled

isobar channels can be eliminated, producing a complex, energy-dependent, effective f matrix in the NN sector. In Ref. 5 the width of an isobar is taken into account for this case by integrating $f_{\rm eff}$ over the Breit-Wigner mass distribution of the isobar. When width effects are important (near threshold) they are treated in this way, replacing the transition potential in that channel with a change of the corresponding f-matrix component. However, over the extended energy region being fitted, the energy dependence of a transition potential can differ significantly from that of boundary condition coupling. In Ref. 5 when both transition-potential effects and width effects are important in the description of a specific coupled system, these aspects were examined separately, but could not be treated together.

The important technical feature of the present work is the use of a code which treats each physical channel, such as the $N\Delta$ system with a given J, L, S, and T, as a large set of channels with distributed isobar masses. The coupling to these channels is weighted by the Breit-Wigner distribution, both for the transition potential and the off-diagonal f-matrix component. Widths and transition potentials are both taken into account appropriately and simultaneously. Of course, this is at the expense of much longer computation times. An added advantage to this approach is that the resulting amplitudes for production of isobars of distributed mass enables the prediction of the decay-product distribution.

In some instances the computation of one-pion-exchange transition potentials to states neglected in Ref. 5 have indicated their importance and we have included them here.

In Sec. II we describe the formalism and calculational methods. In Sec. III we present applications to the $^3P_0$, $^3P_2$-$^3F_2$, $^1D_2$, and $^3F_3$ channels, all of which may have resonances. We also discuss implications for the $^1S_0$ and $^3S_1$-$^3D_1$ channels which have consequences for the lowest-lying six-quark resonances. Section IV summarizes the implications of the results.

II. FORMALISM AND CALCULATIONAL METHOD

The basic formalism for coupled-channel scattering used here has been described in detail in the literature.[5] However, the previous computer program was not able to simultaneously include the effects of the isobar widths and the transition potentials for the coupling of isobar channels to stable hadron channels. When width effects were included, the coupling of these channels was restricted to that due to the off-diagonal f-matrix components at the boundary. We have modified the old program to overcome this deficiency. The price paid is an increase in computer time by an order of magnitude.

A. Coupled-channel equation

We write the coupled-channel equations of Ref. 5 in a form that explicitly represents the distribution of isobar masses as a distribution of channels. We ignore the coupling of the isobar channels to each other as such coupling has only an indirect effect on the observable results and introduces no new qualitative consequences.

We will use an index notation suitable for the two-nucleon reaction which will be the only application presented in this paper. The alteration for scattering of other stable hadron pairs is obvious. Let α, β be the two-nucleon channel indices ($\alpha,\beta=1,2$, for the tensor coupled channels and only 1 otherwise) and let i be the index for isobar channels (channels with either one isobar and one nucleon or with two isobars). We will use κ and λ indices for all the channels, collectively. For the modified partial waves $u_\lambda(r)=r\psi_\lambda(r)$,

$$-\frac{1}{M_\alpha^r}\frac{d^2u_\alpha(r)}{dr^2}+\frac{L_\alpha(L_\alpha+1)}{M_\alpha^r r^2}u_\alpha(r)+\sum_\beta V_{\alpha\beta}(r)u_\beta(r)+\sum_i \tilde{V}_{\alpha i}(r)\int_{m+\mu_i}^{\infty}\varphi_i(M_*,r)dM_*=k_\alpha{}^2u_\alpha(r)\ , \tag{2}$$

where

$$\varphi_i(M_*,r)\equiv[\mathcal{N}_i\rho_i(M_*)]^{1/2}u_i(M_*,r) \tag{3}$$

and, for $M+\mu_i\le M_*<\infty$

$$-\frac{1}{M_{*i}^r}\frac{d^2u_i(M_*,r)}{dr^2}+\frac{L_i(L_i+1)}{M_{*i}^r r^2}u_i(M_*,r)+V_{ii}u_i(M_*,r)+\sum_\alpha \tilde{V}_{i\alpha}(r)[\mathcal{N}_i\rho_i(M_*)]^{1/2}u_\alpha(r)=[k_i(M_*)]^2u_i(M_*,r)\ , \tag{4}$$

M is the nucleon mass and μ_i is m_π or $2m_\pi$ when the isobar decays into a nucleon and one or two pions, respectively (the code also deals with the case of an isobar decaying partly to one pion and partly to two pions by using $\rho=\alpha\rho_\pi+\beta\rho_{\pi\pi}$ where α and β represent the probability of decay into one and two pions, respectively). These equations contain the Breit-Wigner distribution functions

$$\rho_i(M_*)=q_i{}^{2l_i+1}M_*{}^{-2l_i}\left[(\bar{M}_i{}^2-M_*{}^2)^2+\Gamma_i{}^2\frac{\bar{M}_i{}^4}{M_*{}^2}\left[\frac{q_i}{\bar{q}_i}\right]^{4l_i+2}\right]^{-1} \tag{5}$$

and their normalization

$$\mathcal{N}_i^{-1}=\int_{M+\mu_i}^{\infty}\rho_i(M_*)dM_* \ . \tag{6}$$

The k_α, $k_i(M_*)$ and the L_λ are the channel momenta and orbital angular momenta, respectively. The $q_i\equiv q(M_*)$ and the l_i are the relative momenta and orbital angular momenta of the baryon-meson pair arising from the isobar decay (we assume the decay takes place through some two-body system). $\bar{q}_i$ is the q_i corresponding to the central mass M_i of the isobar and Γ_i is the total decay width. Equation (4) is written in a form appropriate to an isobar-nucleon channel. If the channel has two isobars with nonzero width, Eq. (4) must be replaced by a convolution over the two distributions. In our $\Delta\Delta$ channel case we have found[5] that the convolution can be replaced by a single ρ_i with an effective Γ_i and $\overline{M}_i$.

The M_α^r and M_{*i}^r are the reduced masses appropriate to each channel. The $V_{\lambda\kappa}(r)$ are the potentials ($V_{\lambda\kappa}=V_{\kappa\lambda}$) and

$$\tilde{V}_{\lambda\kappa}(r)=\left[\frac{M_\kappa^r}{M_\lambda^r}\right]^{1/2}V_{\lambda\kappa}(r) \tag{7}$$

as required for unitarity[15,18] (this factor was used in the calculations of Ref. 5 although not explicitly indicated in the notation).

Also required are the boundary conditions applied at core radius r_0:

$$r_0\frac{du_\alpha}{dr_0}=\sum_\beta f_{\alpha\beta}u_\beta(r_0)+\sum_i f_{\alpha i}\int_{M+\mu_i}^{\infty}\varphi_i(M_*,r_0)dM_* \tag{8}$$

and

$$r_0\frac{du_i(M_*)}{dr_0}=\sum_\alpha f_{i\alpha}[\mathcal{N}_i\rho_i(M_*)]^{1/2}u_\alpha(r_0)+f_{ii}u_i(M_*,r_0) \tag{9}$$

with $f_{i\alpha}=f_{\alpha i}$.

We note, as in Ref. 5, that when the transition potentials are neglected, one can drop the terms proportional to $\tilde{V}_{\alpha i}$ and $\tilde{V}_{i\alpha}$ in Eqs. (2) and (4), solve Eq. (4) for the outgoing wave functions $u_i^+(M_*,r)$, and insert the result in Eqs. (8) and (9) to obtain

$$r_0\frac{du_\alpha}{dr_0}=\sum_\beta f_{\alpha\beta}^{\text{eff}}u_\beta \ , \tag{10}$$

where

$$f_{\alpha\beta}^{\text{eff}}=f_{\alpha\beta}-\sum_i f_{\alpha i}f_{i\beta}\int_{M+\mu_i}^{\infty}dM_*\frac{\mathcal{N}_i\rho_i(M_*)}{f_{ii}+\theta_i^+(M_*)} \tag{11}$$

with

$$\theta_i^+(M_*)=-\frac{r_0}{u_i^+(M_*,r_0)}\frac{du_i^+(M_*,r)}{dr_0} \ . \tag{12}$$

This considerably simplifies the calculations, but the quadrature in Eq. (11) still takes substantial computer time as the θ_i^+ must be calculated for each M_* used in the integration.

B. Discretization of the width

To solve the above equations numerically without neglect of the $\tilde{V}_{\alpha i}$ and $\tilde{V}_{i\alpha}$, we discretize the width to obtain a finite number of coupled differential equations. In order to discretize the width we substitute for the integration over $\varphi_i(M_*,r)$, in Eqs. (2) and (8), a sum over a distribution of masses. The trapezoidal rule is used for a reason which will become clear:

$$\int_{M+\mu_i}^{\infty}\varphi_i(M_{*,r})dM_* \rightarrow\sum_{j=1}^{n_i}\frac{h_j}{2}[\varphi_i(M_{*j},r)+\varphi_i(M_{*(j+1)},r)] \ , \tag{13}$$

where $h_j=M_{*(j+1)}-M_{*j}$. As a cutoff for the top limit of integration, we use the kinematical restriction $M_*\le(s+M^2)^{1/2}$, with s the invariant mass, which ignores only a negligible portion of the integral. We can then compactly rewrite Eqs. (2), (4), (8), and (9) as

$$-\frac{d^2\bar{u}_\lambda(r)}{dr^2}+\frac{L_\lambda(L_\lambda+1)}{r^2}\bar{u}_\lambda(r)+\sum_{\kappa=1}^{n}\bar{V}_{\lambda\kappa}\bar{u}_\kappa(r)=k_\lambda{}^2\bar{u}_\lambda(r) \tag{14}$$

and

$$r_0\frac{d\bar{u}_\lambda(r)}{dr_0}=\sum_{\kappa=1}^{n}\bar{f}_{\lambda\kappa}\bar{u}_\kappa(r_0) \ , \tag{15}$$

where the λ,κ indices now run over the two-nucleon and all the discretized channels $j_i=1,2,\ldots,n_i+1$ of the m isobar channels labeled by i. Therefore,

$$n=n_0+\sum_{i=1}^{m}(n_i+1)$$

where $n_0=1$ or 2 depending on whether the two-nucleon channel is not or is tensor coupled. We have defined

$$\bar{u}_\alpha(r)=u_\alpha(r) \ , \tag{16a}$$

$$\bar{u}_{\lambda(i,j)}=u_i(M_{*j},r)\left[\frac{H_j}{2}\right]^{1/2} \ , \tag{16b}$$

where

$$H_1=M_{*2}-M_{*1},\quad H_{n_i+1}=M_{*(n_i+1)}-M_{*n_i} \ , \tag{17a}$$

and

$$H_j=M_{*(j+1)}-M_{*(j-1)},\quad j=2,\ldots,n_i \ , \tag{17b}$$

$$\bar{V}_{\lambda,\kappa}=0 \text{ and } \bar{f}_{\lambda,\kappa}=0 \text{ unless } \lambda=\alpha,\beta \text{ or } \kappa=\alpha,\beta \text{ or } \lambda=\kappa \ , \tag{18}$$

$$\bar{V}_{\alpha,\beta}=MV_{\alpha,\beta},\quad \bar{f}_{\alpha,\beta}=f_{\alpha\beta} \ , \tag{19}$$

$$\bar{V}_{\alpha,\lambda(i,j)}=(MM_{*j})^{1/2}[\mathcal{N}_i\rho_i(M_{*j})]^{1/2}\left[\frac{H_j}{2}\right]^{1/2}V_{\alpha i}=\bar{V}_{\lambda(i,j),\alpha} \ , \tag{20}$$

$$\bar{f}_{\alpha,\lambda(i,j)}=[\mathcal{N}_i\rho_i(M_{*j})]^{1/2}\left[\frac{H_j}{2}\right]^{1/2} f_{\alpha,i}$$

$$=\bar{f}_{\lambda(i,j),\alpha} , \tag{21}$$

and

$$\bar{V}_{\lambda(i,j),\lambda(i,j)}=M_{*j}V_{i,i} ,$$

$$\bar{f}_{\lambda(i,j),\lambda(i,j)}=f_{i,i} .$$

In the limit $n\to\infty$, Eqs. (14) and (15) reproduce the results of Eqs. (2), (4), (8), and (9). To minimize the number of coupled channels n for a given accuracy, the M_{*j} are concentrated where the $\rho_i(M_{*j})$ is large. In practice, this is accomplished by using about 15 equally spaced M_{*j} between μ_i and $\bar{M}_i+\Gamma_i$ and two M_{*j} for $M_{*j}>\bar{M}_i+\Gamma_i$. It is important to note that each M_{*j} produces a discrete threshold at the corresponding two-nucleon energy, which produces cusps of magnitude $\propto H_j$ in the phase parameters at these energies. Thus, the phase parameters at these threshold energies have the largest errors, midway between thresholds the phase parameters have errors of the opposite sign and at some offset from these thresholds the phase parameters are exact. The approximate value of this offset is determined by comparison with the results of the old code [see Eqs. (10)–(12)] for the case of vanishing transition potential. In this way, we have obtained accurate results for most of the results in this paper (less than 0.1° in the phase-shift difference and 0.05 in the inelasticity difference from the old code) by using 17 channels to decompose the width of one physical isobar channel. On a VAX 780 the central-processing-unit (CPU) time is about 20 minutes per energy when the width of one physical channel is included.

When the scattering energy is far from the physical threshold region, the influence of the width is small and accurate results are provided by the version of the old code which neglects the width but includes transition potentials. This code only requires about 20 sec of VAX 780 CPU time per energy. It is used where appropriate to save computing time.

III. NUCLEON-NUCLEON SCATTERING RESULTS

A. The $^1D_2$ channel

As shown in Ref. 5, when the Δ width is ignored the strong coupling of the $^1D_2$ NN channel to the $L'=0$, $^5S_2$ $N\Delta$ channel produces a large cusp in the phase shift at inelastic threshold, $T_L=630$ MeV [in general, there is a discontinuity in the $(L'+1)$th derivative at inelastic threshold]. It was also shown that the cusp becomes a broad smooth maximum when the width is included. Although the transition potential then had to be omitted in that work, an adequate fit was obtained within the uncertainty of the experimental phase shifts at that time. Since then there have been new data and the experimental phase shift have changed significantly for $T_L>500$ MeV. Also, the results of different phase shift analyses are now much closer than before.[19–21] Consequently, the fitting requirements are now different and more stringent than they were in Ref. 5.

Apart from using the new code, which allows transition potentials when the isobar widths are taken into account, the present model is more realistic because of the inclusion of the $^5D_2$ $N\Delta$ state. This was omitted in Ref. 5 because of the higher effective threshold due to the angular momentum barrier. However, the one-pion-exchange coupling strength to the two nucleon system is stronger than that of the $^5S_2$ partial wave. Its contribution turns out to be crucial to obtaining the correct fit at $T_L=800$ MeV, as this is the region of the effective threshold for the $N\Delta$ system in a D wave.

The fit to experimental data requires the introduction of two-pion-exchange range transition potentials, to reduce the effect of the one-pion-exchange transition potentials. The potentials resulting from one-pion exchange and the fitted two-pion range terms are

$$V[NN(^1D_2)-N\Delta(^5S_2)]$$
$$=-0.098m_\pi V_2(m_\pi r)+0.335r^{-1}e^{-2m_\pi r} ,$$

$$V[NN(^1D_2)-N\Delta(^5D_2)]$$
$$=0.1176m_\pi V_2(m_\pi r)-1.25r^{-1}e^{-2m_\pi r} ,$$

$$V[N\Delta(^5S_2)-N\Delta(^5S_2)]=-0.079m_\pi V_0(m_\pi r) ,$$

where

$$V_0(x)=x^{-1}e^{-x}$$

and

$$V_2(x)=(x^{-1}+3x^{-2}+3x^{-3})e^{-x} .$$

We note that the effect of the diagonal $N\Delta(^5S_2)$ potential on the $^1D_2$ amplitude is negligible and has been included only for completeness. Other possible coupled channels are unimportant because of high thresholds and weak coupling.

The fit obtained for the phase shift and inelasticity is shown in Figs. 1(a) and 1(b). The curve of $\eta(^1D_2)$ shows the effect of the coupling to the $N\Delta(^5D_2)$ channel. The value continues to decrease sharply after 600 MeV instead of leveling shortly after the 630-MeV threshold. The $^5D_2$ coupling also causes the steep descent of $\delta(^1D_2)$ to continue. These features conform to the data. As shown in Figs. 1(a) and 1(b), the phase shift does not peak as much, nor the inelasticity decrease as rapidly, near $T_L=500$ MeV as the experimental values. If the phase-shift analyses are accurate this may indicate that there is some continuum, nonisobaric, pion production contributing significantly below the N-Δ threshold.

In the Argand plot, Fig. 2, it is seen that the model and data both indicate the rapid counterclockwise motion typical of an inelastic resonance.

B. The $^3F_3$ channel

The $^3F_3$ channel can couple to $N\Delta$ in $P(L'=1)$ and $F(L'=3)$ waves, to $\Delta\Delta$ in P, F, and $H(L'=5)$ waves, and to NN^* in an F wave. However, all the other one-pion-exchange interactions are relatively small compared to the coupling to $N\Delta(^5P_3)$. Furthermore, the other ef-

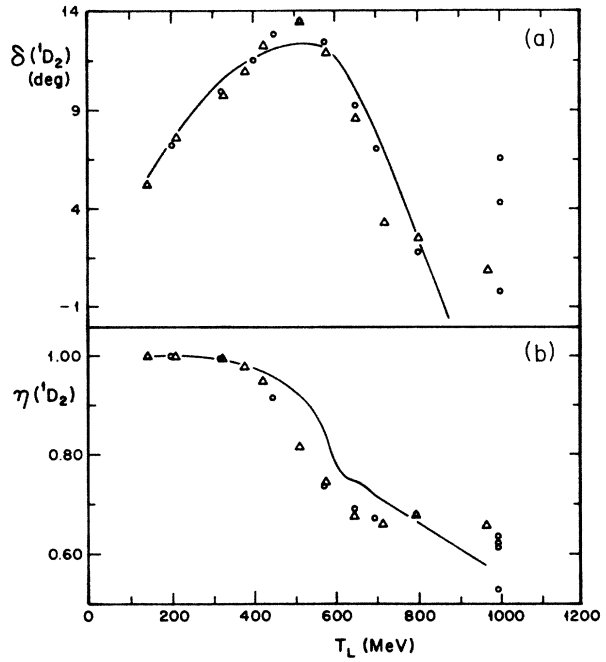

FIG. 1. (a) The $^1D_2$ phase shift. The open triangles denote the phase-shift analysis of Ref. 19. The open circles denote the analysis of Ref. 21. The solid curve is the model prediction for $NN(^1D_2)$ coupled to $N\Delta(^5S_2)$ and $N\Delta(^5D_2)$ with f-matrix elements $f_{NN,NN}=19.3$, $f_{NN,N\Delta(S)}=0.2$, $f_{NN,N\Delta(D)}=1.5$, $f_{N\Delta(S),N\Delta(S)}=1.0$, $f_{N\Delta(S),N\Delta(D)}=f_{N\Delta(D),N\Delta(D)}=0.0$. (b) The $^1D_2$ inelasticity. The points and curve denote phase-shift solutions and model prediction as in (a).

fective thresholds are also higher so that one expects the dominant effects to come from the $N\Delta(^5P_3)$ coupling. However, for the higher energies in the range considered, i.e., say, $T_L > 700$ MeV, and as confirmed below by our fit, the influence of extra channels can start to be important. We only use the one-pion-exchange interactions:

$$V[NN(^3F_3)-N\Delta(^5P_3)]=-0.1288 m_\pi V_2(m_\pi r)\ ,$$

$$V[N\Delta(^5P_3)-N\Delta(^5P_3)]$$
$$=-0.079 m_\pi V_0(m_\pi r)+0.0063 m_\pi V_2(m_\pi r)\ .$$

As in the $^1D_2$ case, the diagonal potential has no influence whatsoever. No two-pion-exchange interaction is needed. The fit to new phase shifts, Fig. 3(a), is very good, a much better fit than that of Ref. 5 or Ref. 22 at the peak and beyond. For the inelasticity, Fig. 3(b), our result is too elastic above 700 MeV, in the region at which there can be some effect from higher-mass coupled channels. It is difficult at this point to predict which of these extra channels are going to be most important until we have more inelastic experimental data available for these energies and beyond. However, one is tempted to some speculation. Looking at the different couplings, it turns out that the most favored channels are $N\Delta(^5F_3)$ and $N\Delta(^3F_3)$. Their couplings to $NN(^3F_3)$ are only one-half to one-third of that to $N\Delta(^5P_3)$, but their influence increases with energy since their thresholds are higher.

We make a technical remark concerning this case. In the region around $T_L=500$ MeV, the instability of the numerical results with respect to the mass offset chosen

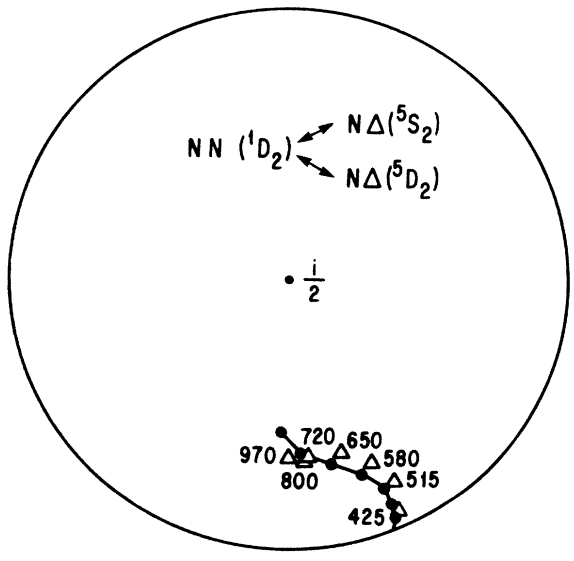

FIG. 2. Argand plot for the $^1D_2$ amplitude. The points and solid curve are denoted as in Fig. 1(a). The filled circles on the model denote the same energies as the open triangles. The laborabory energies T_L are indicated in MeV.

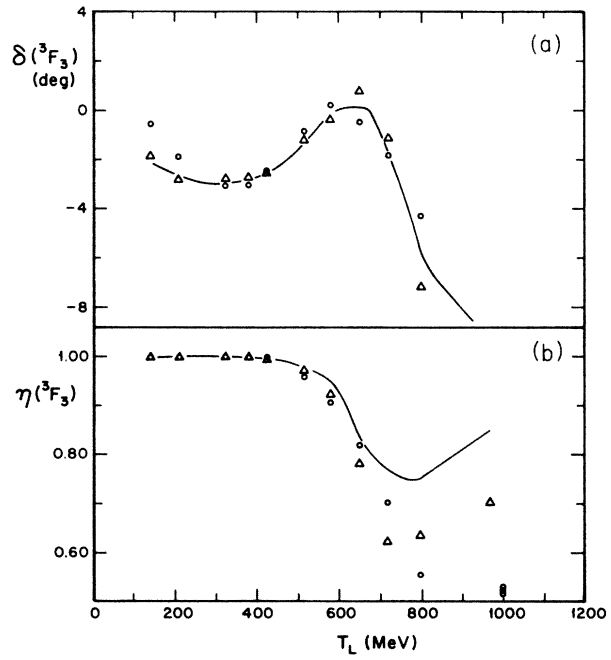

FIG. 3. (a) The $^3F_3$ phase shift. The phase-shift analysis points and solid curve are denoted as in Fig. 1(a). The model curve corresponds to $NN(^3F_3)$ coupled to $N\Delta(^5P_3)$ and $f_{NN,NN}=5.4$, $f_{NN,N\Delta}=2.72$, $f_{N\Delta,N\Delta}=0.3$. (b) The $^3F_3$ inelasticity. Points and curve are denoted as in (a).

has made it necessary to increase the number of channels and consequently the computing time to obtain enough accuracy,

The Argand plot, Fig. 4, shows the counterclockwise rotation of an inelastic resonance beginning at $T_L=425$ MeV although it is not as strong as that of the $^1D_2$ case.

C. The $^3P_0$ channel

The $^3P_0$ nucleon-nucleon channel is of interest because both the experimental data[21,23] and some models[5,22] indicate that it, like the $^1D_2$ and $^3F_3$ channels, may be resonant at low energies. The uncertainty is due to the inelasticity which varies greatly in the phase-shift analyses and depends on short-range coupling in the model. The subject is discussed in Ref. 22 in which a model that has a slight counterclockwise rotation in the Argand plot is compared with data. But that model, using the old code, did not include the effect of transition potentials. The width had to be taken into account as the inelastic structure, if it exists, is at $T_L<630$ MeV.

We first remark that in the fits of Refs. 5 and 22, $\delta(^3P_0)$ is somewhat too large for $T_L<210$ MeV. This is not sensitive to the channel coupling but represents a deficiency in the Feshbach-Lomon nucleon-nucleon potential. This is rectified here by using $g_{NN\pi}{}^2/4\pi=13.0$ but may represent a deficiency of the semirelativistic two-pion potential of Ref. 17.

The $N\Delta(^3P_0)$ channel is the only channel to which the $NN(^3P_0)$ can couple which has both the lowest threshold energy and the lowest L' available. The one-pion transition potential has moderate strength:

$$V[NN(^3P_0)-N\Delta(^3P_0)] = 0.1467 m_\pi V_0(m_\pi r)-0.0733 m_\pi V_2(m_\pi r)\ .$$

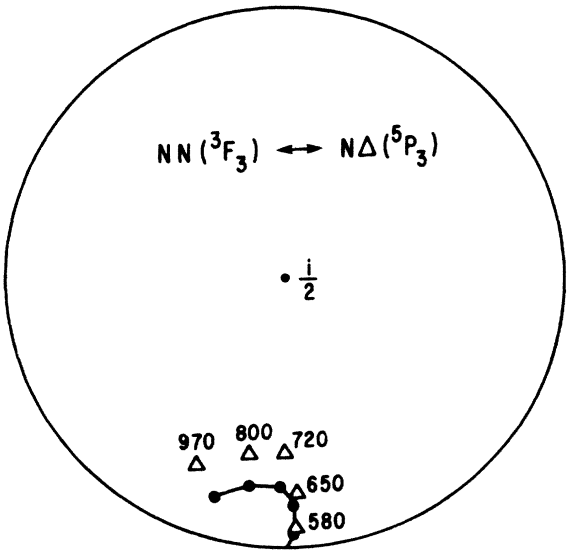

FIG. 4. Argand plot for the $^3F_3$ amplitude. Notation as in Fig. 2. f-matrix parameters as in Fig. 3(a).

We do not use a two-pion range potential for this case. No other $N\Delta$ channel can couple. Therefore, all the remaining coupled channels have a higher threshold energy. We present, in Figs. 5(a) and 5(b), two fits which differ only in the strength of coupling at the boundary. The less strongly coupled, $f_{NN,N\Delta}=0.3$, fits the phase parameters of Ref. 19 well, and the other, $f_{NN,N\Delta}=2.0$, fits the phase parameters of Ref. 21 [except for η at $T_L\geq 800$ MeV which would require an assist from the $\Delta\Delta(^3P_0)$ and $NN^*(^3P_0)$ coupling].

Examining the Argand plots [Figs. 6(a) and 6(b)] we see that the slope of the amplitude is significantly different when the two different couplings are used. For the less strongly coupled case it clearly rotates clockwise. However, for the more strongly coupled case between $T_L=580$ and 800 MeV, the Argand plot is nearly straight and may have a slightly counterclockwise rotation. The confirmation of a possible structure in this partial wave awaits data for $T_L>600$ MeV which is sensitive to $\eta(^3P_0)$. This could be $d\sigma/d\Omega$ (absolute) together with A_{XX}, A_{ZZ}, and D in the elastic data, or detailed single-pion production data.

D. The $^3P_2$-$^3F_2$ channel

While the older phase-shift analysis of this channel gave no indication of structure (see Ref. 5), recent analyses[19–21] have indicated a rapid drop in $\eta(^3P_2)$ for

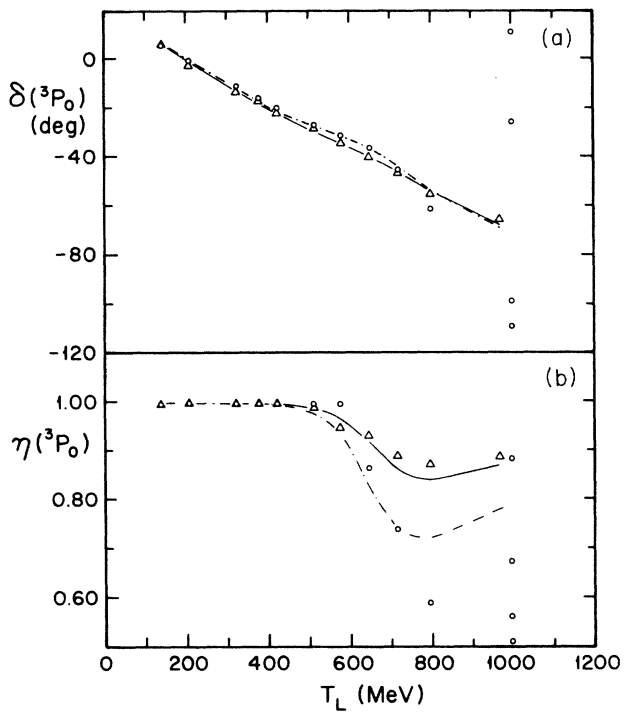

FIG. 5. (a) The $^3P_0$ phase shift. The points denote phase-shift solutions as in Fig. 1(a). The solid and dash-dot curves are the model predictions for $NN(^3P_0)$ coupled to $N\Delta(^3P_0)$. The solid curve corresponds to $f_{NN,NN}=25.0$, $f_{NN,N\Delta}=-0.3$, $f_{N\Delta,N\Delta}=-0.2$. The dash-dot curve corresponds to $f_{NN,NN}=26.0$, $f_{NN,N\Delta}=-2.0$, $f_{N\Delta,N\Delta}=-0.2$. (b) The $^3P_0$ inelasticity. Points and curves are denoted as in (a).

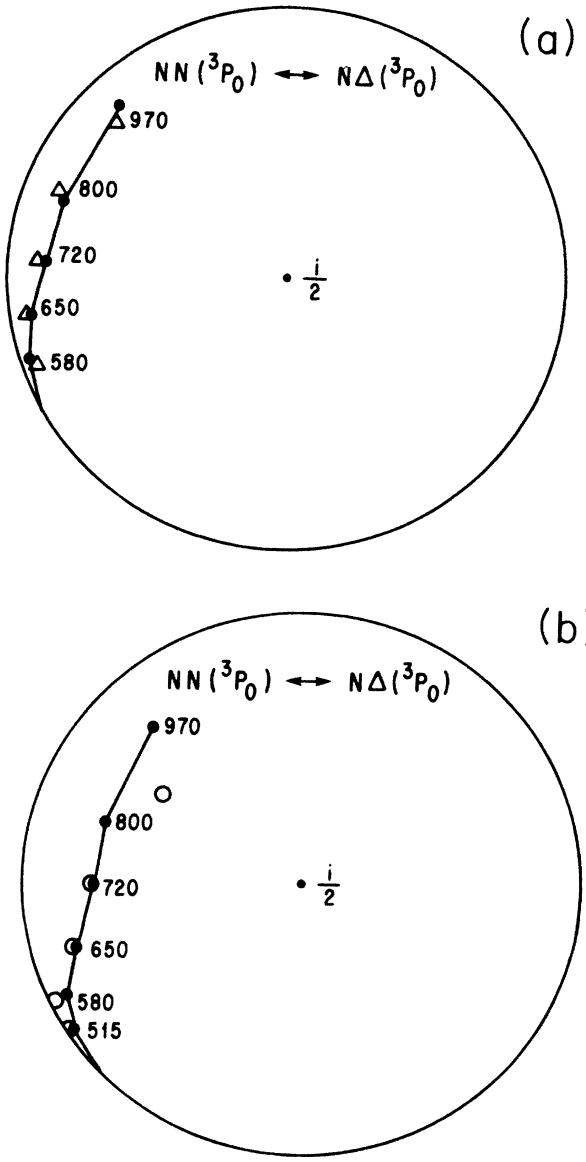

FIG. 6. (a) Argand plot for the $^3P_0$ amplitude. Notation as in Fig. 2. The model corresponds to $f_{NN,NN}=25.0$, $f_{NN,N\Delta}=-0.3$, $f_{N\Delta,N\Delta}=-0.2$. (b) Argand plot for the $^3P_0$ amplitude. Notation as in Fig. 2. The model corresponds to $f_{NN,NN}=26.0$, $f_{NN,N\Delta}=-2.0$, $f_{N\Delta,N\Delta}=-0.2$.

$T_L > 600$MeV and a decreasing $\delta(^3P_2)$ for $T_L > 800$ MeV (Refs. 19 and 21) or even for $T_L > 600$ MeV (Ref. 20). We note that the model of Ref. 5 was forced to produce these features for $T_L > 650$ MeV in order to fit the lower-energy data. We now show that these features persist with our more realistic model and that a resonance is predicted in the vicinity of 1000 MeV.

First, we realize that, apart from the $N\Delta(^3P_2)$ channel considered in Ref. 5, other channels have important one-pion-exchange transition potentials to the $^3P_2$-$^3F_2$ NN channel. In particular, $N\Delta(^5P_2)$, $N\Delta(^5F_2)$, and $N\Delta(^3F_2)$ are of some significance. It is possible to combine the effects of the two P-wave or the two F-wave isobar channels using Eq. (31) of Ref. 5. It turns out that the resulting potentials provide too much coupling. As the boundary coupling has little effect on P waves at low energy, the way to get a fit to experimental data is to cancel some of the one-pion-exchange effect with two-pion-exchange contributions of opposite sign. We have found as the adequate final potentials, including the one-pion-exchange terms obtained as indicated above:

$$V[NN(^3P_2)-N\Delta(P)] = -0.068 m_\pi V_2(m_\pi r)+1.65 r^{-1} e^{-2m_\pi r},$$

$$V[NN(^3F_2)-N\Delta(P)] = -0.0762 m_\pi V_2(m_\pi r)+1.3 r^{-1} e^{-2m_\pi r},$$

$$V[NN(^3P_2)-N\Delta(F)] = 0.154 m_\pi V_2(m_\pi r)-3.5 r^{-1} e^{-2m_\pi r},$$

$$V[NN(^3F_2)-N\Delta(F)] = 0.116 m_\pi V_2(m_\pi r)-2.0 r^{-1} e^{-2m_\pi r}.$$

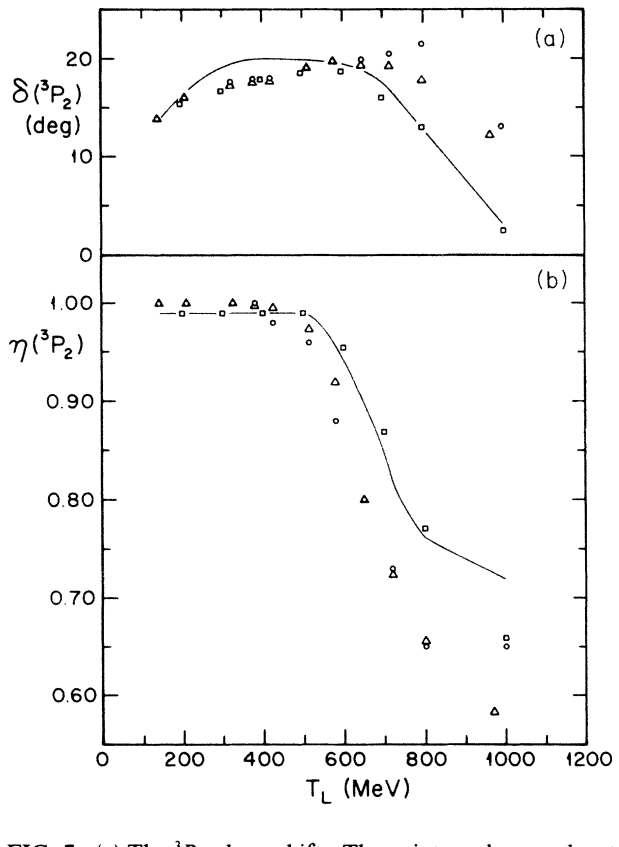

FIG. 7. (a) The $^3P_2$ phase shift. The points and curve denote phase-shift solutions as in Fig. 1(a). The open squares denote the single-energy phase-shift analysis SP85 of Ref. 20. The solid curve is the model prediction for $NN(^3P_2)$ coupled to $NN(^3F_2)$ (via the NN tensor potential) and to $N\Delta(^{3,5}F_2)$ and $N\Delta(^{3,5}P_2)$. $f_{PP}=1.73$, $f_{PF}=-0.9$, $f_{P,N\Delta(F)}=-2.12$, $f_{P,N\Delta(P)}=0.8$, $f_{FF}=40.0$, $f_{F,N\Delta(F)}=f_{F,N\Delta(P)}=f_{N\Delta(F),N\Delta(F)}=f_{N\Delta(F),N\Delta(P)}=0.0$, $f_{N\Delta(P),N\Delta(P)}=0.1$. (b) The $^3P_2$ inelasticity. The points and curve are denoted as in (a).

With this choice we get a good fit to $\delta(^3P_2)$, $\eta(^3P_2)$, by tuning $f_{NN(^3P_2)-N\Delta(P)}$, with $f_{NN(^3P_2)-NN(^3P_2)}$ correlated, to give the low-energy $\delta(^3P_2)$ values. The results are shown in Figs. 7 and 8. As in Ref. 5, the $\delta(^3F_2)$ fit is poor and is significant for $L=3$. In Figs. 9(a) and 9(b) we represent the coupling parameter ϵ_2 and the mixing angle ϕ_2 given by the model. The fit for ϵ_2 is reasonable.

The Argand plot for the $^3P_2$ complex phase, Fig. 10, shows the counterclockwise behavior of an inelastic resonance from $T_L > 800$ MeV.

E. Comments on the $^1S_0$ and $^3S_1$-$^3D_1$ channels

The complex models required for the $^1S_0$ and $^3S_1$-$^3D_1$ channels will be the subject of a forthcoming paper,[24] which will also consider the effect of interior quark states.[2,9,10] However, a few remarks of interest may be made now.

Because the $NN(^1S_0)$ couples only to the $N\Delta$ system in the $^5D_0$ channel, it is important to consider the coupling to the $\Delta\Delta$ and $NN^*(1440)$ systems in spite of their greater threshold energy. In both of the latter systems there is coupling to the $^1S_0$ state whose effective threshold is not far above that of the $N\Delta(^5D_0)$ channel. The resultant fit to the elastic nucleon-nucleon scattering data presented in Ref. 5 is quite good.

In that fit the Δ width is included in the $N\Delta(^5D_0)$ channel (whose threshold is in the experimental region) and consequently the transition potential to that channel

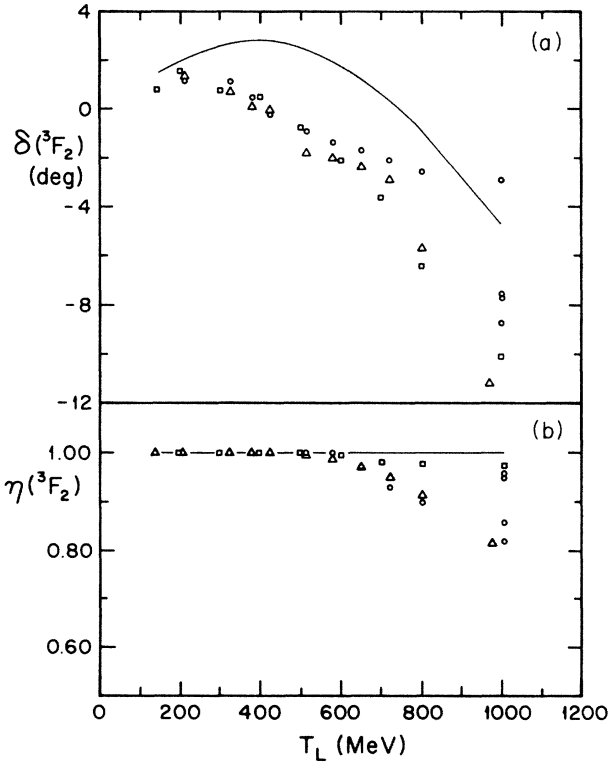

FIG. 8. (a) The $^3F_2$ phase shift. The points and curve are denoted as in Fig. 7(a). (b) The $^3F_2$ inelasticity. The points and curve are denoted as in Fig. 7(a).

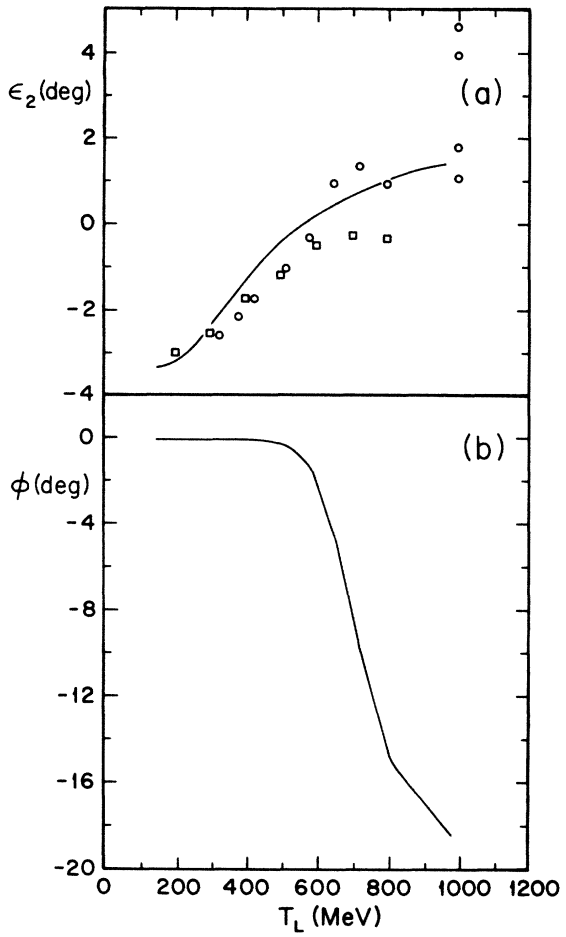

FIG. 9. (a) The $J=2$ coupling parameter ϵ_2. Notation as in Fig. 7(a). (b) The mixing angle ϕ_2 predicted by the model as a function of the energy.

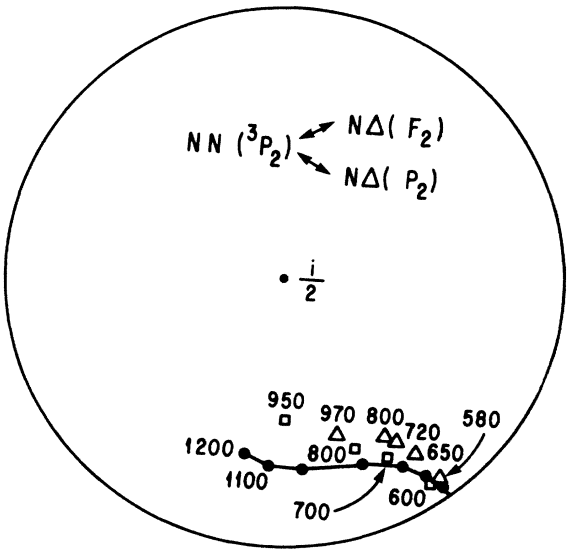

FIG. 10. Argand plot for the $^3P_2$ amplitude. Notation as in Figs. 2 and 7(a). The corresponding energies are made explicit.

is ignored. The transition potentials to the $\Delta\Delta(^1S_0)$ and $NN^*(^1S_0)$ channels are included. Estimates of the inelasticity to the latter two channels near $T_L = 800$ MeV were made later[25] by ignoring the transition potentials and suitably modifying the boundary coupling. This showed that the two-pion production generated by these channels exceeded the data[26] by two orders of magnitude. Subsequent work with the old code[25] showed that one could modify the short-range coupling to the two-pion channels so as to agree with the experimental production limit.

We now find similar effects with the new code, in which the comparison with both the low-energy pion production and the elastic-scattering phase shifts can be made consistently. The distortion of the phase shifts by the width of the higher-mass channels is substantial, in addition to the effect on the inelasticity parameter. In the forthcoming paper[24] we will consider the sensitivity of the projections to higher energy (and the six-quark resonances) to the choice of boundary couplings and of QCD models.

The $^3S_1$-$^3D_1$ nucleon-nucleon system is particularly complex. Although isospin conservation forbids any $N\Delta$ channel, the $\Delta\Delta(^3S_1)$, $\Delta\Delta(^3D_1)$, $\Delta\Delta(^7D_1)$, and $NN^*(^3S_1)$ channels can all be expected to have significant roles. The $\Delta\Delta(^7D_1)$ has a particularly strong one-pion-exchange coupling and cannot, therefore, be ignored compared to the lower effective threshold $\Delta\Delta(^3S_1)$ and $NN^*(^3S_1)$. The $\Delta\Delta(^3D_1)$ must also be included because of its important role in the deuteron elastic magnetic form factor.[27–29] The large Δ magnetic moment and the opposing spin and orbital angular momentum alignments of the $^7D_1$ and $^3D_1$ $\Delta\Delta$ states have important consequences for that form factor. The consequences of various balances between the coupling to the four isobar channels mentioned, for both the deuteron[27,28] and the six-quark resonances,[10] will be discussed.[24,29] In particular, total coupling strength to the $\Delta\Delta(^7D_1)$ state is strongly restricted by deuteron data.[27–29]

IV. CONCLUSIONS

We have constructed realistic models for nucleon-nucleon scattering partial waves at intermediate energies by using meson-exchange potentials and short-range, energy-independent boundary conditions with explicit coupling to the low orbital angular momentum $N\Delta$, $\Delta\Delta$, and $NN^*(1440)$ channels. They provide good descriptions of the physics of all the nucleon-nucleon channels that are nontrivial for $T_L \leq 1$ GeV. The spreading of the threshold effects by the Breit-Wigner mass distributions of the isobars is very important in fitting the data, as is the large scale energy dependence due to the one-pion range transition potentials. As before,[5] the characteristic increase of attraction (or decrease of repulsion) below threshold, followed by a sharp decrease in the phase shift and a minimum in inelasticity above threshold,[30] is important in fitting the physical data. This critical behavior is not obtained by including the coupling to intermediate states in the derivation of an adiabatic nucleon-nucleon potential.[31,32] The best way to get an accurate representation of this energy dependence is to explicitly couple channels using potential (and boundary condition) matrices.

We have reinvestigated the $^3P_0$, $^3P_2$-$^3F_2$, $^1D_2$, and $^3F_3$ two-nucleon systems with transition potentials and width simultaneously taken into account, and with extra isobar channels where indicated. These more realistic models provide improved fits to the analyzed phase parameters[19–21] (some of which have changed significantly from those available during the preparation of Ref. 5). The results confirm the coupled-channel nature of the $^1D_2$ and $^3F_3$ structures. There is no need to attribute these structures to exotic six-quark states, nor does such a model describe the data well.[2,3]

Confirmation of the existence of the previously inferred structure in the $^3P_0$ channel[5,21–23] is shown to require more experimental information on the inelasticity parameter. That parameter determines the short-range coupling strength which, in turn, determines the structure. A previous prediction of coupled-channel structure in the $^3P_2$ channel, [5] near $T_L = 800$ MeV, is confirmed, and is close to that indicated by the recent phase-shift analyses.[19–21]

The present method allows us to develop improved models for the $^1S_0$ system and examine the consistency with the measured two-pion production cross section at $T_L = 800$ MeV (Ref. 26). The $^3S_1$-$^3D_1$ model is being extended to be consistent with deuteron properties, including the sensitive magnetic from factor.[27–29] Both of these, together with the improved $^1D_2$ system model, will provide a more reliable extrapolation of these phase parameters to the region[2] where six-quark f-matrix poles affect these states. The size of these effects will be more closely predicted.[24]

The improved models for all of the nucleon-nucleon partial waves enable more reliable predictions of the magnitude of observable effects produced by the six-quark f poles, as these depend on interference between the resonant and nonresonant states.[9,10] The better extrapolation to higher energies will, in general, help identify the most sensitive experiments for accurate phase-shift analyses.

An important advantage of the present calculation over that of Ref. 5 is that it predicts the S-matrix elements for the production of isobars as a function of the isobar mass. One can then predict, through the subsequent decay of the isobars, the observable distributions in the $NN\pi$ and $NN\pi\pi$ final states.[1,33] We plan to do this in collaboration with the authors of Ref. 1. The comparison with production data will further restrict our coupled-channel models. The relative strength of coupling to different isobar channels is often poorly determined by comparison with the elastic data, but is very sensitive to production data.

ACKNOWLEDGMENTS

One of us (E.L.L.) benefited from the hospitality and facilities of the Los Álamos National Laboratory, the University of Paris, University College, London, the University of California at Los Angeles, and the University of Washington, Seattle, during the preparation of this paper. This work was supported in part by funds provided by the U.S. Department of Energy (DOE) under Contract No. DE-AC02-76ER03069. The other author would like to thank the Fulbright program for financial support.

*On leave of absence from the Departamento de Física Teórica, Valencia, Spain.

[1]J. Dubach, W. M. Kloet, and R. R. Silbar, Phys. C **33**, 373 (1986); R. R. Silbar, J. A. Tjon, E. E. van Faassen, J. Dubach, and W. M. Kloet, in *Hadronic Probes and Nuclear Interactions,* proceedings of the conference, Arizona State University, 1985, edited by J. R. Comfort, W. R. Gibbs, and B. G. Ritchie (AIP Conf. Proc. No. **133**) (AIP, New York, 1985), p. 398.

[2]E. L. Lomon, Nucl. Phys. A **434**, 139c (1985); in *Hadron Substructure in Nuclear Physics,* proceedings of the Workshop, Indiana University, 1983, edited by W. Y. P. Hwang and M. H. Macfarlane (AIP Conf. Proc. No. 110) (AIP, New York, 1984), p. 117.

[3]I. P. Auer *et al.*, Phys. Rev. Lett **41**, 1436 (1978); **41**, 354 (1978); K. Hidaka and A. Yokosawa, Surv. High Energy Phys. **1**, 141 (1980).

[4]P. J. Mulders, A. T. Aerts, and J. J. deSwart, Phys. Rev. D **21**, 2653 (1980).

[5]E. L. Lomon, Phys. Rev. D **26**, 576 (1982).

[6]W. M. Kloet and R. R. Silbar, Nucl. Phys. **A338**, 281 (1980); **A338**, 317 (1980); Phys. Rev. Lett. **45**, 970 (1980).

[7]T.-S. H. Lee, Phys. Rev. Lett. **50**, 1571 (1983).

[8]J. A. Tjon and E. E. van Faassen, Phys. Rev. C **30**, 285 (1984).

[9]E. L. Lomon, in *Proceedings of the 6th International Symposium on High Energy Spin Physics, Marseille, 1984,* edited by J. Soffer [J. Phys. (Paris) Colloq. **46**, C2-329 (1985)].

[10]P. LaFrance and E. L. Lomon, Phys. Rev. D **34**, 1341 (1986).

[11]H. Goldberg and E. L. Lomon, Phys. Rev. **131**, 120 (1963); **134**, B659 (1964).

[12]M. Krammer and E. L. Lomon, Phys. Rev. Lett. **20**, 71 (1968).

[13]R. H. Dalitz and S. F. Tuan, Ann. Phys. (N.Y.) **10**, 307 (1960).

[14]E. L. Lomon and C. L. Yen, Bull. Am. Phys. Soc. **8**, 21 (1963).

[15]S. Hirschi, Ph.D. thesis, MIT, 1970.

[16]H. Feshbach and E. L. Lomon, Ann. Phys. (N.Y.) **29**, 19 (1964).

[17]E. L. Lomon and H. Feshbach, Ann. Phys. (N.Y.) **48**, 94 (1968).

[18]M. H. Partovi and E. L. Lomon, Phys. Rev. D **2**, 1999 (1970).

[19]D. V. Bugg, private communication; older results are in R. Dubois *et al.*, Nucl. Phys. **A377**, 554 (1982).

[20]R. A. Arndt *et al.*, Phys. Rev. D **28**, 97 (1983). We are using the phase-shift solution SP85 available by computer access to Scattering Analysis Interactive Dial-in (SAID) at Virginia Polytechnic Institute and State University.

[21]J. Bystricky *et al.*, Report No. DPhPE82-12 (unpublished); J. Bystricky, in *Proceedings of the 6th International Symposium on High Energy Spin Physics* (Ref. 9), p. C2-487.

[22]E. L. Lomon, Phys. Rev. D **31**, 1746 (1985).

[23]I. P. Auer *et al.*, Phys. Rev. D **29**, 2435 (1984); G. R. Burleson *et al.*, Nucl. Phys. **B213**, 365 (1983).

[24]P. Gonzalez, P. LaFrance, and E. L. Lomon (in preparation).

[25]J. A. Minahan, B.Sc. thesis, MIT, 1982.

[26]F. H. Cverna *et al.* Phys. Rev. C **23**, 1698 (1981).

[27]E. L. Lomon, *Proceedings of Tenth International Conference on Few Body Problems in Physics, Karlsruhe, 1983,* edited by B. Zeitnitz (North-Holland, Amsterdam, 1983), Vol. II, p. 83.

[28]P. Sitarski, B.Sc. thesis, MIT, 1985.

[29]P. Blunden, P. Sitarski, and E. L. Lomon (in preparation).

[30]E. L. Lomon, Phys. Rev. D **1**, 549 (1970).

[31]W. N. Cottingham *et al.*, Phys. Rev. D **8**, 800 (1973); M. Lacombe *et al.*, Phys. Rev. C **21**, 861 (1980).

[32]R. Machleidt, Physics **197**, 352 (1984); Ch. Elster, K. Holinde, and R. Machleidt (in preparation).

[33]A. I. Miller and E. L. Lomon, Phys. Rev. D **2**, 1245 (1970).